Stratospheric versus Tropospheric Control of the Strength and Structure of the Brewer–Dobson Circulation

EDWIN P. GERBER

Center for Atmosphere Ocean Science, Courant Institute of Mathematical Sciences,
New York University, New York, New York

ABSTRACT

The strength and structure of the Brewer–Dobson circulation (BDC) are explored in an idealized general circulation model. It is shown that diabatic forcing of the stratosphere and planetary wave forcing by the troposphere can have comparable effects on tracer transport through the stratosphere, as quantified by the mean age of air and age spectrum. Their impact, however, is mediated through different controls on the mass circulation. Planetary waves are modulated by changing surface topography. Increased wave forcing strengthens the circulation, particularly at lower levels. This is primarily a tropospheric control on the BDC, as the wave forcing is set by stationary waves at the base of the stratosphere. Stratospheric control of the circulation is effected indirectly through the strength of the stratospheric polar vortex. A colder vortex creates a waveguide higher into the stratosphere, raising the breaking level of Rossby waves and deepening the circulation. Ventilation of mass in the stratosphere depends critically on the depth of tropical upwelling, and so mass and tracer transport is comparably sensitive to both tropospheric and stratospheric controls.

The two controls on the circulation can lead to separate influences on the lower and upper stratosphere, with implications for the seasonal cycle of tropical upwelling. They allow for independent changes in the "shallow" and "deep" branches of the BDC, which may be important for comparing modeled trends with observations. It is also shown that changes in the BDC have a significant impact on the tropical cold point (on the order of degrees) and the equator-to-pole gradient in the tropopause (on the order of a kilometer).

1. Introduction

The Brewer–Dobson circulation (BDC) characterizes the transport of mass through the stratosphere, a slow upwelling in the tropics, poleward drift through the midlatitudes, and descent in the middle and high latitudes. Dobson et al. (1929) first speculated on the existence of this transport based on the positive equator-to-pole gradient in stratospheric ozone in the boreal spring, a gradient seemingly at odds with the (then) hypothesis that ozone is produced by solar radiation. Unfortunately the conjecture was initially abandoned, and it was not until further measurements of water vapor and helium by Brewer (1949) that sufficient evidence was established. In concert with radiative and chemical processes, the Brewer–Dobson circulation sets the distribution of ozone and water vapor in the middle atmosphere (e.g., Dobson 1956). Stratospheric ozone changes have played an order one role in observed circulation trends to date, shifting the tropospheric jet stream in the Southern Hemisphere (e.g., Thompson and Solomon 2002; Arblaster and Meehl 2006; Polvani et al. 2011). Likewise, Solomon et al. (2010) show that changes in stratospheric water vapor have had a significant impact on observed surface warming. Understanding and simulating the BDC is thus critical for interpreting changes in stratospheric water vapor and ozone in recent decades, and will continue to be so for projections of future climate (e.g., Perlwitz et al. 2008; Son et al. 2008; McLandress et al. 2011).

In this paper, we study the factors that control the strength and structure of the Brewer–Dobson circulation, focusing on the joint roles of the stratosphere and troposphere in shaping mass transport in the stratosphere. To build a bridge between conceptual models of the BDC (e.g., Dunkerton 1989; Holton et al. 1995) and comprehensive simulations with stratosphere-resolving atmospheric models (e.g., McLandress and Shepherd 2009),

Corresponding author address: Edwin P. Gerber, Center for Atmosphere Ocean Science, Courant Institute of Mathematical Sciences, 251 Mercer Street, New York, NY 10012.
E-mail: gerber@cims.nyu.edu

we study the transport in an idealized general circulation model (GCM). The model, developed by Polvani and Kushner (2002) and Gerber and Polvani (2009), simulates the primitive equation dynamics of the atmosphere with the same fidelity as comprehensive models, therefore capturing the nonlinear interactions between planetary and synoptic waves with the mean flow, but with an idealized forcing that allows us to systematically vary both tropospheric and stratospheric conditions. A key conclusion of our study is that both tropospheric wave forcing and stratospheric diabatic forcing can have equal impacts on mass and tracer transport in the middle to upper stratosphere.

The extremely long time scales of the BDC, on the order of years for much of the stratosphere, prohibit direct measurement of the circulation. In addition, the Lagrangian circulation outside the deep tropics is primarily effected by eddies, and so is best quantified by the residual mean circulation of the transformed Eulerian mean (TEM) equations (Edmon et al. 1980; Andrews et al. 1987). As established in the downward control principal by Haynes et al. (1991), the circulation outside of the deep tropics is mechanically driven by wave-induced torques. Downward control allows one to estimate the Lagrangian mean circulation indirectly from the heating generated by vertical motion—which can be estimated from direct measurements—and so provides a means for quantifying the observed BDC (e.g., Rosenlof 1995). As discovered by Brewer (1949) and Dobson (1956), however, the BDC is fundamentally connected to the transport of chemical species. The estimate of the Lagrangian transport in the TEM circulation captures the diabatic circulation (i.e., the transport of mass across isentropic surfaces) but does not account for the mixing of tracers along isentropes (e.g., Plumb 2002). Tracer transport by the BDC is therefore more directly related to the mean age of air and age spectrum (Waugh and Hall 2002). These measures quantify the length and variability of transport pathways through the stratosphere.

To connect tracer transport to the Lagrangian circulation, we compare tracer-based calculations of the age spectrum with the residual mean circulation. We probe the impact of changes in the tropospheric wave forcing on the BDC by altering the surface orography of the model, and the impact of changes of the diabatic forcing in the stratosphere by varying the cooling of the winter polar vortex. As would be expected from downward control theory, increased planetary wave forcing increases the amplitude of the residual mean circulation. Tracer transport follows the circulation changes, and the mean, modal, and spectral width of the age spectrum decrease. We term the impact of the planetary wave forcing "tropospheric control" of the BDC, as it is largely independent of

stratospheric conditions. Given that the BDC is primarily mechanically forced, however, the impact of diabatic forcing in the stratosphere may be less intuitive. The structure of the polar vortex has relatively little direct impact on the net diabatic transport into and out of the stratosphere, but it controls the distribution of wave breaking, and so the depth of the residual circulation. In terms of tracer transport, however, this has an equally important impact on the age spectrum statistics in the mid- to upper stratosphere. We term this influence of stratospheric conditions "stratospheric control" of the BDC, as it is largely independent of the planetary wave forcing from the troposphere below.

The relative independence of these two controls provides a possible mechanism for structural changes in the Brewer–Dobson circulation. As suggested by Plumb (2002, Fig. 2), there are conceptual grounds for distinguishing the BDC into "shallow" and "deep" branches. The former characterizes the strong circulation in the lowermost stratosphere where synoptic wave breaking plays a significant role, and the latter a weaker circulation high into the stratosphere, driven primarily by planetary waves originating from the high latitudes. This conceptual distinction was put on firmer ground by Birner and Bönisch (2011), who find a separation in the mean transit times of the mass circulation in the lower and upper stratosphere. Bönisch et al. (2011) present observational evidence for a recent increase in the shallow BDC that may have occurred independent of any change in the deep circulation above. We find that changes in tropospheric wave driving, coupled with changes in stratospheric diabatic forcing, can indeed lead to distinct changes in BDC in the upper and lower stratosphere.

In studying the circulation with an idealized GCM, we have omitted the impact of small-scale (10–1000 km) gravity waves. Such "unresolved" gravity waves play a significant role in stratospheric circulation, driving roughly 10%–25% of the stratospheric circulation in comprehensive models (e.g., Eyring et al. 2010, ch. 4). We have chosen to focus on the resolved circulation in this study to establish a reproducible, conceptual framework. As gravity waves are the primary driver of the circulation in the mesosphere, we focus only on the stratospheric circulation where resolved waves dominate. Future work will explore the impact of gravity wave parameterizations in the idealized GCM. Initial tests have suggested, however, that there is a substantial degree of compensation between resolved and parameterized waves.

In section 2, we describe the model and introduce the primary diagnostics of the paper, the mean age of air, age spectrum, and residual mean circulation. Section 3 presents the key result of the paper, highlighting the difference between tropospheric and stratospheric control

of the Brewer–Dobson circulation. This conceptual framework is developed in detail in sections 4 and 5, where we explore the impact of model parameters on the diabatic circulation and connect these changes to the tracer transport, respectively. Potential impacts of the BDC on climate are presented in section 6, where we focus on changes in the tropopause and tropical cold point, and section 7, where we discuss the potential for structural changes in the circulation. We summarize our results and conclude in section 8.

2. Model and methods

A series of perpetual-January integrations with an idealized GCM form the core of the study. The runs are nearly identical to those presented in Gerber and Polvani (2009). The model is a pseudospectral dynamical core developed by the Geophysical Fluid Dynamics Laboratory (GFDL) and forced with a highly simplified physical parameterization, as described by Held and Suarez (1994) and modified by Polvani and Kushner (2002), to produce a realistic circulation in the stratosphere and troposphere. We refer the reader to these papers for the precise details of the forcing but review the most important features here.

The key simplification to the model physics is in the temperature equation, where all diabatic processes are approximated by Newtonian relaxation to an analytic, radiative–convective equilibrium–like profile. This allows the model to produce a fairly realistic mean circulation without radiation or convection schemes. In the troposphere, the profile is exactly as in Held and Suarez (1994) except that a gradient in temperature is introduced between the two hemispheres to mimic solstitial conditions. In the stratosphere, temperature in the summer hemisphere and tropics is relaxed to the U.S. Standard Atmosphere. In the winter hemisphere, a polar night jet is forced by reducing the temperature of the equilibrium profile. Over the polar cap, the equilibrium profile decreases in height with specified lapse rate γ (K km^{-1}). The vortex lapse rate γ is a key parameter in this study. As it is increased, the winter stratosphere grows colder and polar vortex becomes stronger.

The second key variable in this study is the surface topography. As only planetary-scale waves extend deep into the stratosphere, Gerber and Polvani (2009) showed that a very simple surface topography was sufficient to excite an active stratospheric circulation. Surface topography of wavenumber k and amplitude h_0 is added in the winter hemisphere between 25° and 65°N. Gerber and Polvani (2009) found that the most realistic stratosphere–troposphere coupling was found in simulations with $\gamma = 4$ and topographic wavenumber $k = 2$ and amplitude $h_0 = 3$ km.

The Polvani and Kushner (2002) GCM includes a crude parameterization of mesospheric gravity wave drag by introducing a Rayleigh friction above 0.5 hPa, acting on the five uppermost layers of the model, which extend to approximately 0.01 hPa. Drag near the model top is necessary to slow down the polar night jet, as the winds in radiative equilibrium exceed several hundred meters per second at these altitudes. This crude parameterization, however, introduces a nonconservative drag in the uppermost atmosphere. Shepherd and Shaw (2004) show that this can effect the stratospheric and tropospheric circulations through downward control. The negative effects are most pronounced in "low top" models with an upper boundary within the stratosphere (e.g., 10 hPa), as documented by Shaw et al. (2009). Aware of this potential weakness in our model, we have taken care to ensure that all the results in this study are not affected by the upper boundary condition.

Table 1 lists the integrations used in this study. All were integrated for 10 000 days after a 300-day spinup period. Circulation-based metrics converged much faster than this, but long integrations were necessary to quantify the tracer transport. The integrations with $\gamma = 0$, however, are singular in that there is almost no ventilation of the upper stratosphere above 10 hPa. We avoid analysis of tracer transport in the upper stratosphere in these integrations, as convergence here is extremely slow. Integrations were run at T42 resolution (triangular truncation at wavenumber 42), with 40 sigma ($\sigma = p/p_s$. where p is pressure and p_s surface pressure) layers spaced evenly in height z, as in Polvani and Kushner (2002). Tracers are modeled in grid space and advected with a finite-volume parabolic scheme. The robustness of the model to resolution and numerics has also been investigated, and will be presented in greater detail in a future paper. We find that the residual mean circulation of the model at T42L40 resolution is very robust to changes in resolution and numerics, as confirmed in simulations with a finite-volume dynamical core with a cubed sphere grid. Tracer transport, on the other hand, is sensitive to model numerics and resolution, as found by Eluszkiewicz et al. (2000). The tracer-based results shown in this paper are qualitatively robust, but the quantitative age of air is sensitive to numerics.

Metrics

The "mean age" of stratospheric air and the "age spectrum" quantify the transport times of tracers through the atmosphere. These measures can be directly related to stratospheric chemistry processes, as the time air has been in the stratosphere quantifies how long it has been exposed to ultraviolet radiation and stratospheric reactions (e.g., Waugh and Hall 2002). Formally, the mean age $\Gamma(x)$ at a point x in the atmosphere quantifies the

TABLE 1. Details of the integrations presented in this study. We have grouped the integrations into parameter sweep experiments; thus a few integrations have been listed multiple times for clarity. In the last column, we highlight the figure(s) in which the integration is presented.

N	γ (K km^{-1})	k	h_0 (km)	Figure(s)
1	4	—	0	1–5, 9–13
2	4	2	1	4–7, 9, 10, 12, 13
3	4	2	2	4–6, 9, 10, 12–14
4	4	2	3	4–6, 9, 10, 12, 13
5	4	2	4	1–7, 9–13
6	4	1	1	6, 10
7	4	1	2	6, 10
8	4	1	3	6, 10
9	4	1	4	6, 10
10	4	1	5	6, 10
9	4	1	4	(see above)
5	4	2	4	(see above)
11	4	3	4	10
12	4	4	4	10
13	0	2	3	4–6, 8–10, 12, 13
14	1	2	3	4–6, 9, 10, 12, 13
15	1.5	2	3	1–3, 10, 11
16	2	2	3	4–6, 8–10, 12–14
17	3	2	3	4–6, 9, 10, 12, 13
4	4	2	3	(see above)
18	5	2	3	1–6, 9–13
19	6	2	3	4–6, 8–10, 12, 13
20	0	—	0	10
21	2	—	0	10
1	4	—	0	(see above)
22	6	—	0	10

average time it takes air to get there from the surface, specified as a boundary Ω. To compute the age, one must integrate over all possible pathways from the surface Ω to x, accounting for both advection and the quasi-horizontal mixing of air parcels along isentropes. Hence in practice we use a tracer to estimate the age, thus capturing all the relevant processes. The mean age in the stratosphere is on the order of years, compared with on the order of days throughout the troposphere, where air is continually in contact with the surface.

The age spectrum provides further information on the pathways taken by air from Ω to x. As established by Hall and Plumb (1994), the age spectrum can be viewed as a Green's function $\mathcal{G}(x|\Omega, t)$, which propagates tracer mixing ratio from Ω to x in time t. The mean age is then just the first moment of the age spectrum:

$$\Gamma(x) = \int_0^\infty t \mathcal{G}(x|\Omega, t) \, dt. \tag{1}$$

Following Waugh and Hall (2002), we quantify the key features of the age spectrum with the spectral width Δ and the "modal age." The spectral width quantifies the spread of the spectrum, that is, the variance of the different paths the tracer takes from the boundary to x. It is related to the second moment of the age spectrum:

$$\Delta^2(x) = 1/2 \int_0^\infty [t - \Gamma(x)]^2 \mathcal{G}(x|\Omega, t) \, dt. \tag{2}$$

The modal age, the mode of the age spectrum, quantifies the most likely transit time.

We obtain the age spectrum by computing the "boundary impulse response" with a pulse tracer (e.g., Hall et al. 1999). Given the stationary forcing of our model, this provides a fairly good estimate of the actual age spectrum. We compute the mean age two ways, with a "clock tracer" and by taking the mean of the age spectrum, confirming that both yield approximately the same mean age. The clock tracer is a conserved tracer whose concentration near the surface is forced to increase linearly with time. The mean age is then proportional to the difference in concentration of the clock tracer at height and the surface. For both the pulse and clock tracer, we define Ω to be the three lowermost σ surfaces, the surface layer of the Held and Suarez (1994) forcing. For plotting purposes, we show the age relative to the age of the youngest air entering the tropical stratosphere at 100 hPa, to minimize any impacts of the topography on tracer transport in the troposphere below.

The residual mean, or transformed Eulerian mean, circulation approximates the net Lagrangian transport of mass through the atmosphere (e.g., Andrews and McIntyre 1976). It can also be viewed as an approximation, in geometric coordinates, to the zonal mean circulation averaged in isentropic coordinates (e.g., Held and Schneider 1999). As the residual mean circulation accounts for the transport of mass across isentropes, it is referred to as the diabatic circulation, and we adopt this convention for the remainder of the paper. The residual mean meridional and pressure velocities ($\overline{v}^*, \overline{\omega}^*$) and streamfunction ψ^* are defined by

$$\overline{v}^* = \overline{v} - \frac{\partial(\overline{v'\theta'}/\overline{\theta}_p)}{\partial p} = \frac{\partial \psi^*}{\partial p} \tag{3}$$

and

$$\overline{\omega}^* = \overline{\omega} + \frac{1}{a\cos\phi} \frac{\partial(\cos\phi \overline{v'\theta'}/\overline{\theta}_P)}{\partial \phi} = -\frac{1}{a\cos\phi} \frac{\partial(\psi^* \cos\phi)}{\partial \phi}, \tag{4}$$
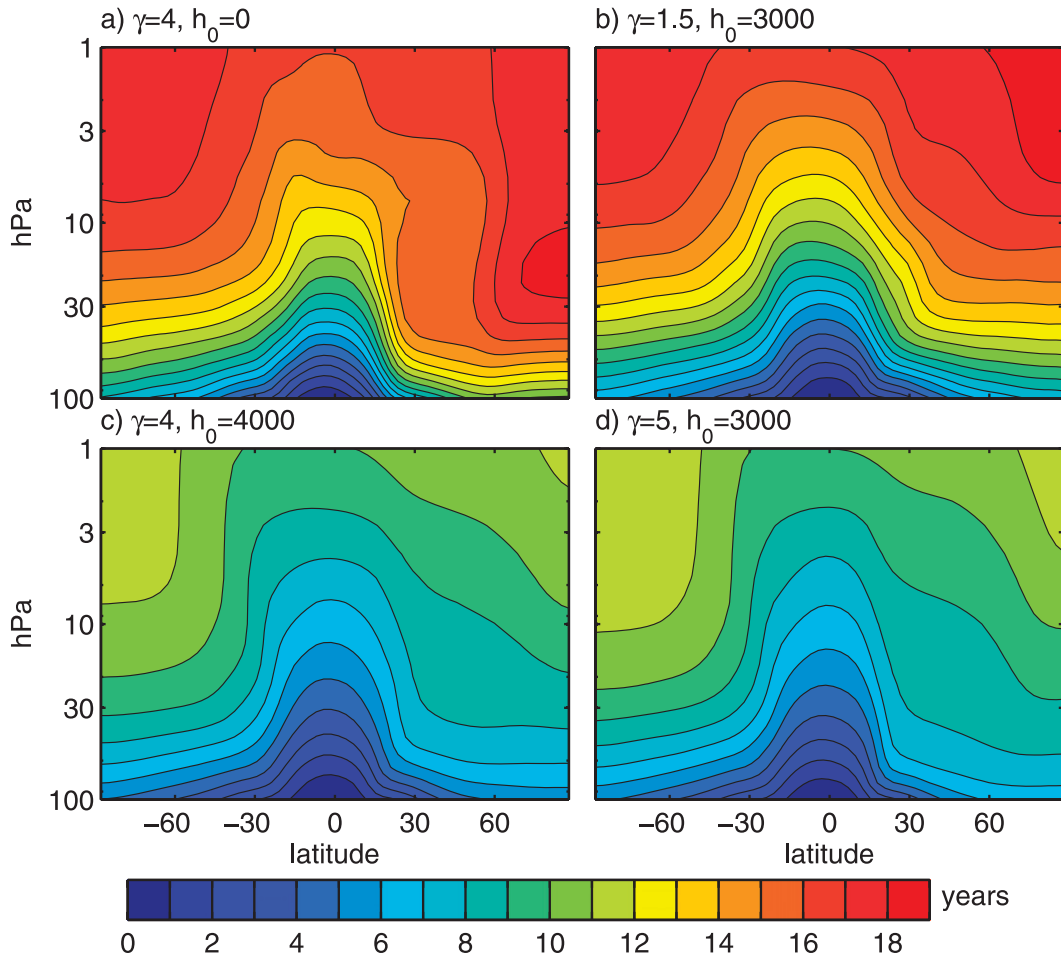
FIG. 1. The mean age of air in four integrations of the idealized model, contrasting (a),(b) two with a very "old" stratosphere and (c),(d) two with a very "young" stratosphere. The two integrations in (a) and (c) differ only in the surface topography, while those in (b) and (d) differ only in the strength of the vortex lapse rate parameter. Wavenumber-2 topography was used in all integrations, and the parameter h_0 is specified in meters. The panels correspond to integrations (a) 1, (b) 15, (c) 5, and (d) 18.

where an overbar and prime denote the zonal mean and deviations therefrom, and v, ω, θ, and ϕ are the meridional wind, pressure velocity, potential temperature, and latitude. As can be seen from (3) and (4), the residual mean streamfunction can be computed directly from the heat flux $\psi^* = \psi + \overline{v'\theta'}/\overline{\theta}_p$, where ψ is Eulerian mean streamfunction. From this perspective, the residual circulation characterizes the Eulerian circulation plus an eddy transport.

3. Tropospheric versus stratospheric control

We begin by exploring two controls on the Brewer–Dobson circulation. The mean age of stratospheric air in four integrations of the idealized GCM is shown in Fig. 1. Tracer transport through the stratosphere is extremely slow in the integrations shown in Figs. 1a and 1b, the

mean age almost 19 yr in the upper stratosphere. In the integrations illustrated in Figs. 1c and 1d, the air is substantially younger, the oldest air now only 11 yr old. The "freshening" of the stratosphere between the two integrations on the left was effected by introducing surface topography to the model. Both integrations were run with a strong polar vortex (equilibrium lapse rate parameter $\gamma = 4$), but in Fig. 1a there is no topography, whereas Fig. 1c was driven with wavenumber-2 topography of amplitude 4 km.

The topography, however, is the same in the two integrations on the right. Here the reduction in mean age was effected by changing the thermal forcing of stratosphere, increasing the equilibrium lapse rate of the stratospheric polar vortex from $\gamma = 1.5$ K km^{-1} in Fig. 1b to 5 K km^{-1} in Fig. 1d. The similarity between the integrations on the left and right suggests that radiative
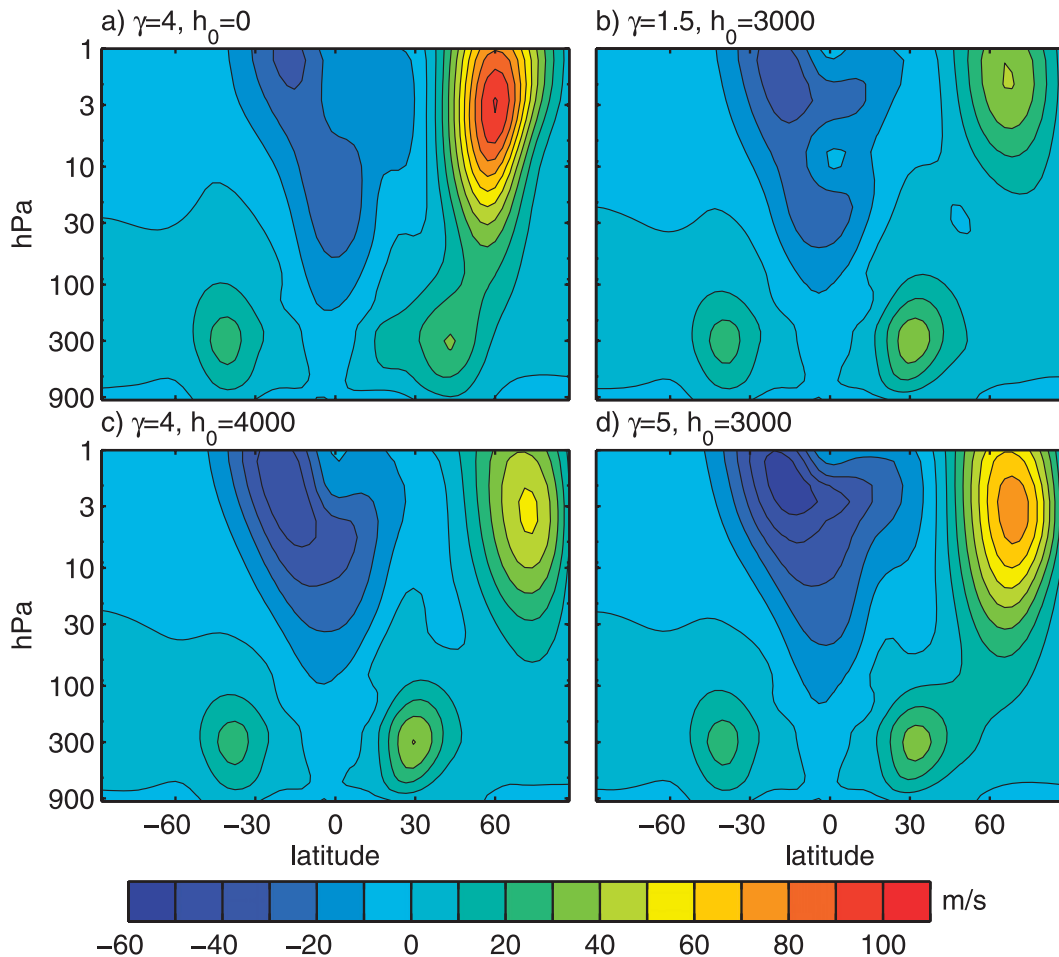
FIG. 2. As in Fig. 1, but for the time and zonal mean zonal wind. Note that the vertical axes have been changed to show the troposphere as well.

changes in the stratosphere can have almost the same effect on the mean age as substantial changes in the wave forcing.

Figure 2 shows the zonal wind climatology of the same four integrations, highlighting the fact that topography and stratospheric thermal forcing have very different impacts on the circulation of the atmosphere, despite the similarity of their influence on the mean age. Of the two "old" integrations in Figs. 2a and 2b, the simulation without topography has a much stronger polar vortex. Weaker diabatic forcing combined with increased planetary wave driving weakens the polar vortex in the integration in Fig. 2b compared with Fig. 2a, as discussed by Gerber and Polvani (2009). The climatologies of the two "young" integrations shown in Figs. 2c and 2d also vary considerably; here, however, the strength of the vortex varies in the opposite sense. Weaker thermal forcing, combined with increased topography, weakens the jet in the integration shown in Fig. 2c relative to that in Fig. 2d.

Figure 2 suggests that the mean age of stratospheric air can be varied distinctly from the climatology: there is not a simple one-to-one relationship between vortex strength and mean age.

One can begin to understand the impact of the two parameters by comparing the residual mean circulations, shown in Fig. 3. While the mean age is similar in the top and bottom integrations, respectively, the residual circulations are significantly different. Focusing first on the "old" integrations in Figs. 3a and 3b, we see that the total amplitude of the circulation, measured as the net upwelling at 100 hPa, is substantially larger in the integration in Fig. 3b, with weak a vortex and topography, than in the integration in Fig. 3a with a strong vortex but no topography. Near the stratopause, at 1 hPa, however, the circulation of the latter simulation is stronger. A similar contrast exists between the two "younger" integrations in Figs. 3c and 3d. While the net residual circulation at 100 hPa is weaker in Fig. 3d compared
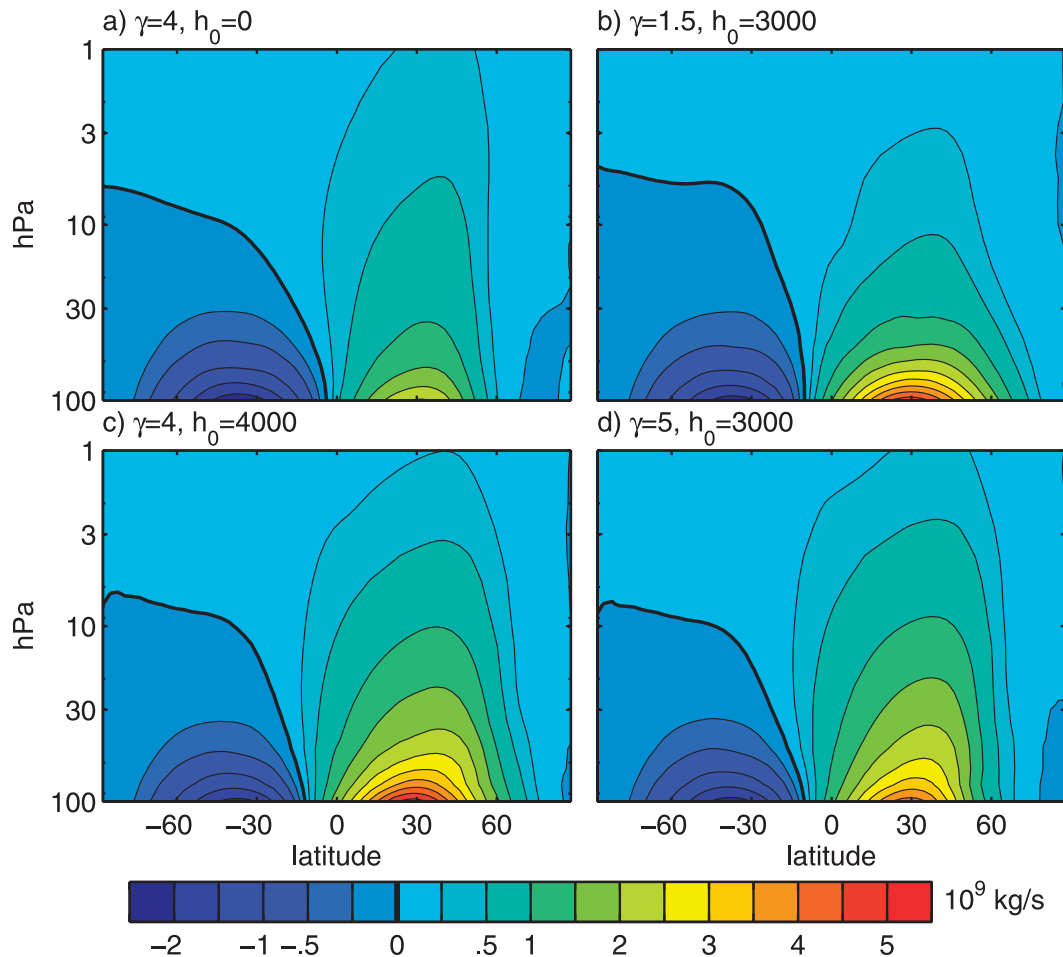
FIG. 3. As in Fig. 1, but for the residual mean mass streamfunction. The contour interval is 0.5×10^9 kg s^{-1}, except that we have included contours at $\pm 0.25 \times 10^9$ kg s^{-1} to highlight the circulation in the upper stratosphere. The zero contour is thick.

with Fig. 3c, the circulation in this integration extends deeper into the stratosphere. Viewed in terms of the differences between the top and bottom integrations, we find that mean age can be reduced by increasing (cf. Figs. 3a,c) or deepening (cf. Figs. 3b,d) the residual circulation.

These four integrations suggest two controls on the Brewer–Dobson circulation. A first critical factor is the amplitude of the planetary wave forcing of the stratosphere. We term this influence "tropospheric control," as we will show that the planetary wave forcing is primarily set by topography and the tropospheric jet structure. The impact of surface topography fits well with our understanding of the BDC as a mechanically driven circulation (e.g., Haynes et al. 1991; Holton et al. 1995). A second control is the diabatic forcing of the polar stratosphere, here approximated by changes in the radiative equilibrium profile controlled by γ. Figure 1 demonstrates

that both factors can have a similar impact on tracer transport through the stratosphere.

4. Controls on the diabatic circulation

To better understand how tropospheric and stratospheric conditions influence stratospheric tracer transport, we first systematically explore changes in the diabatic circulation. Figure 4 shows the residual mean pressure velocity at 10 and 100 hPa for two series of integrations in which the topographic amplitude and vortex lapse rate parameter are systematically varied. Beginning in the lower stratosphere (Figs. 4c,d), we see that topography has a larger impact on the net mass transport into and out of the stratosphere. With larger topography, upwelling (downwelling) increases uniformly between approximately 30°S and 20°N (20°–90°N). There is little change in the Southern Hemisphere (SH) extratropics,
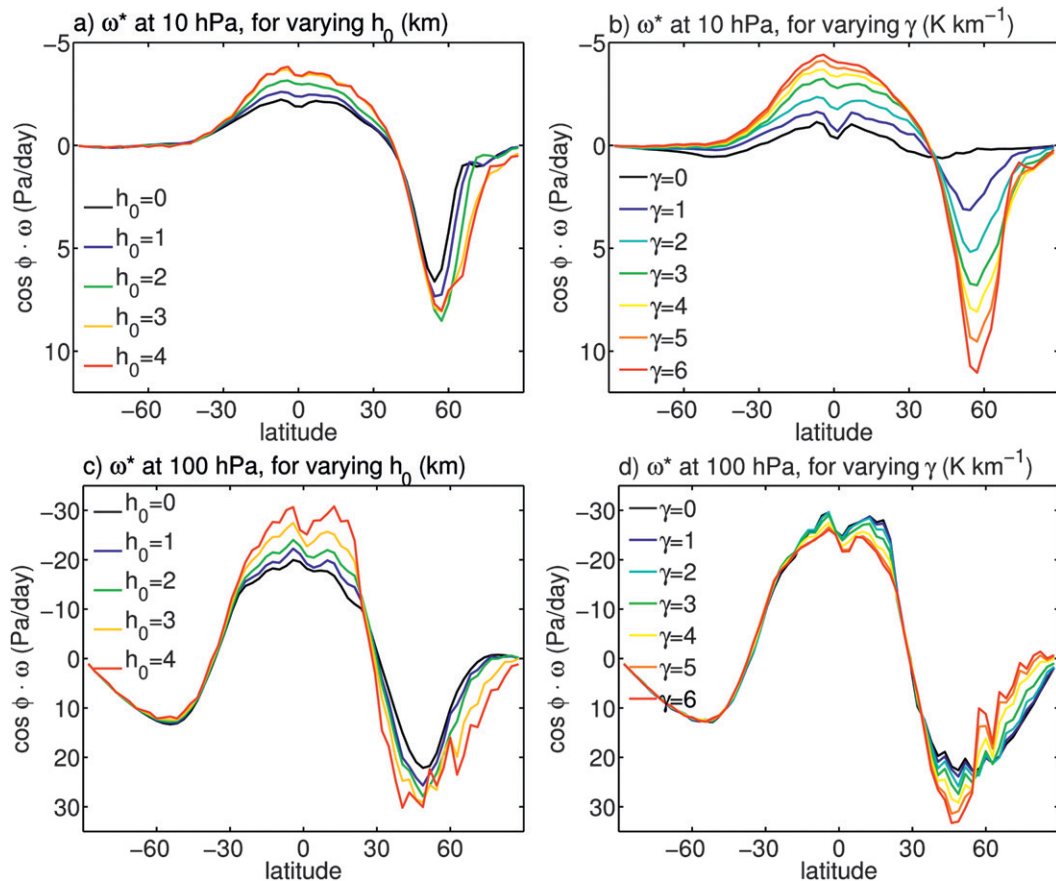
FIG. 4. The residual mean pressure velocity at (a),(b) 10 and (c),(d) 100 hPa. The integrations in (a) and (c) differ only in the amplitude of wavenumber-2 topography at the surface, and the vortex lapse rate parameter is fixed at 4 K km^{-1}. In (b) and (d) the surface topography is fixed, with wavenumber 2 and amplitude 3 km, and γ is varied. Note that while topography has a similar impact on the circulation at both levels, the vortex strength has the opposite impact at 10 and 100 hPa.

as the topography is only in the Northern Hemisphere (NH), but the tropical signal is quite uniform. Clearly planetary wave activity in the NH alone is modulating upwelling throughout the entire tropical stratosphere. This supports the conclusions of Yulaeva et al. (1994), who relate colder temperatures in the lower tropical stratosphere in boreal winter relative to austral winter to greater stationary wave forcing in the NH.

At 100 hPa, changes in the thermal forcing have less of a net impact. Inspection of the tropics indicates that increasing the strength of the polar vortex reduces the upwelling. Increasing γ also shifts the downwelling toward the edge of the polar vortex, increasing it near 50°N and weakening it poleward of 60°N. This is consistent with theoretical expectations based on Charney and Drazin (1961): strong winds in the cold vortex will limit the upward propagation of stationary waves into the vortex, reducing the net wave driving above. This is partially compensated, however, by increased wave driving and downwelling on

the edge of the vortex, where the winds are not as strong. The shift in the circulation in response to changes in the winds highlights the need to account for the latitudinal structure of the winds, as explored in section 4b.

At 10 hPa, the impact of topography on $\overline{\omega}^*$ is about the same as at 100 hPa; increased planetary wave forcing increases vertical motion, although there is some saturation for large values of h_0. The impact of vortex strength, however, is qualitatively different. The vertical motion at this level scales almost linearly with γ: increasing the strength of the vortex increases the diabatic circulation. This confirms the deepening of the circulation suggested in Figs. 3b and 3d.

We relate changes in the diabatic circulation to changes in the resolved wave forcing in Fig. 5. Figures 5a and 5b capture the essential impacts of topography and γ on the residual mean circulation, showing the net downwelling in each hemisphere as a function of height. By downward control, the net mass transport across at
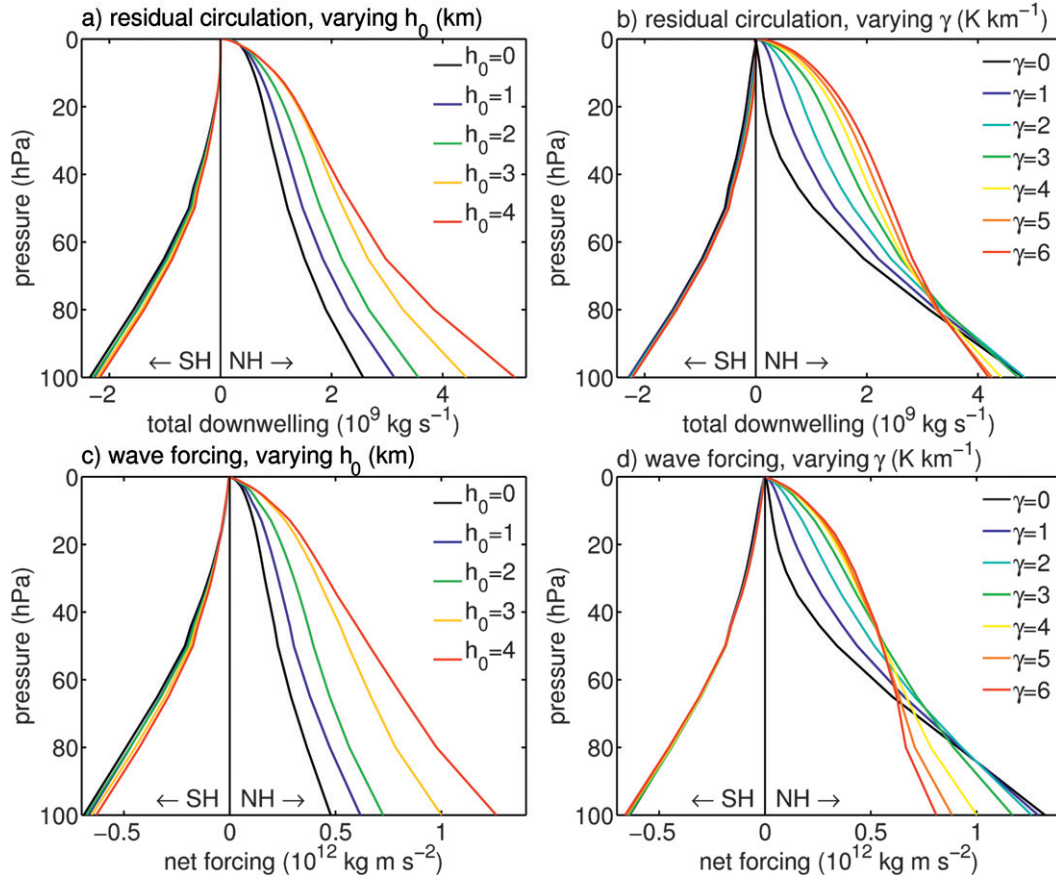
FIG. 5. The vertical structure of the residual circulation and wave driving. The total downward mass flux as a function of height for integrations in which the (a) topography and (b) cooling of the polar vortex are varied. The sign of the mass transport is reversed in the Northern Hemisphere for clarity. As the net upwelling in the tropics must balance to the downwelling in both hemispheres, the total transport by the residual circulation at each pressure level can be inferred from horizontal distances between the SH and NH curves. (c),(d) The total integrated wave forcing from the top of the atmosphere to each pressure level, τ from (5), for the same integrations. Again, the sign is reversed in the NH. While the topography primarily controls the total amplitude of the wave driving, the vortex lapse rate controls its shape.

a given pressure level is a function of the wave forcing above it (Haynes et al. 1991). We confirm this relationship in the model integrations in Figs. 5c and 5d, which illustrate the total wave driving in each integration. Specifically, for each hemisphere we plot

$$\tau(p) = \frac{2\pi r_0^2}{g} \int_{\text{pole}}^{\text{equator}} f \frac{\overline{v'\theta'}}{\overline{\theta}_p} \cos^2\phi \, d\phi, \qquad (5)$$

the net Eliassen–Palm (E-P) flux of wave activity across a pressure surface p. As any net wave activity that propagates across a given pressure level must break above it, this measure is related to the net torque on the atmosphere above each pressure level. The torque is negative, or easterly, in both hemispheres, but we reverse the sign in the NH for clarity.

In Fig. 5a, we see that increasing the topography uniformly increases the diabatic circulation throughout the stratosphere, though changes saturate in the upper stratosphere for increasingly large topography. This follows the increase in wave driving throughout the stratosphere shown in Fig. 5c. Increasing the vortex strength, however, primarily affects the depth of the upwelling, as seen in Fig. 5b. At 80 hPa, there is almost no effect on the upwelling; below this point, a colder vortex reduces the circulation, but above, it increases the circulation. This can be related to the redistribution of wave breaking illustrated in Fig. 5d. Increasing γ allows waves to propagate higher into the stratosphere, increasing wave breaking at upper levels, which in turn deepens the diabatic circulation.

The relationship between the diabatic circulation and the wave forcing is not perfect in Fig. 5 because we have

neglected the horizontal structure of the wave driving. Because of the weakening of the Coriolis force at lower latitudes, the same torque can effect a larger circulation if it is shifted equatorward. Hence the meridional transport of momentum by eddy fluxes also affects the transport. Downward control calculations (not shown) confirm that the differences in upwelling can be fully explained by changes in wave driving. These calculations also allow us to ensure that our results are not skewed by the Rayleigh friction near the model top. We find that the sponge layer response to changes in the wind structure has little effect on the transport. The impact is minimal in simulation with varying topography. Increasing γ does increase the circulation driven by the sponge layer, but the changes are a factor of 10 or more smaller than those driven by changes in resolved wave driving at 10 hPa, and matter less lower in the stratosphere.

a. Tropospheric control

The impact of increased surface topography on the BDC on the model is in keeping with our general understanding of the stratospheric circulation (e.g., Holton et al. 1995). One would expect larger topography to excite larger stationary waves, so increasing the wave forcing and driving a stronger diabatic circulation. This initial impression is correct, provided one is careful to specify where the stationary waves are larger. As shown in Fig. 6a, increasing the topographic forcing increases the amplitude of the stationary wave at the base of the stratosphere. In the stratosphere itself, however, the wave amplitude does not scale with the topography: initially it increases with h_0, reaching a maximum for $h_0 = 2$ km, and then drops down again, so that above 10 hPa the wavenumber-2 amplitude is smaller for $h_0 = 4$ km than for $h_0 = 1$ km. The increased circulation and wave forcing observed in Figs. 5a and 5c is well correlated with the stationary wave amplitude in the upper troposphere and lower stratosphere, but not with the wave amplitude within the stratosphere.

The surface topography controls the amplitude of the standing waves in the troposphere, but in the stratosphere, vortex conditions also play a role in the wave amplitude, as can be seen in Fig. 6b, where the surface topography is fixed at $h_0 = 3$ km and γ is systematically varied. For fixed topography, a colder vortex creates a resonant cavity in the stratosphere leading to stronger stationary waves (e.g., Matsuno 1970). When the vortex forcing is kept constant, however, the stationary waves generated by topography have a nonlinear impact on the vortex. As discussed by Gerber and Polvani (2009), topography reduces the amplitude of the vortex, having a similar effect as γ on the mean state.

To understand the wave amplitude, one must account for wave propagation and reflection (e.g., Harnik and
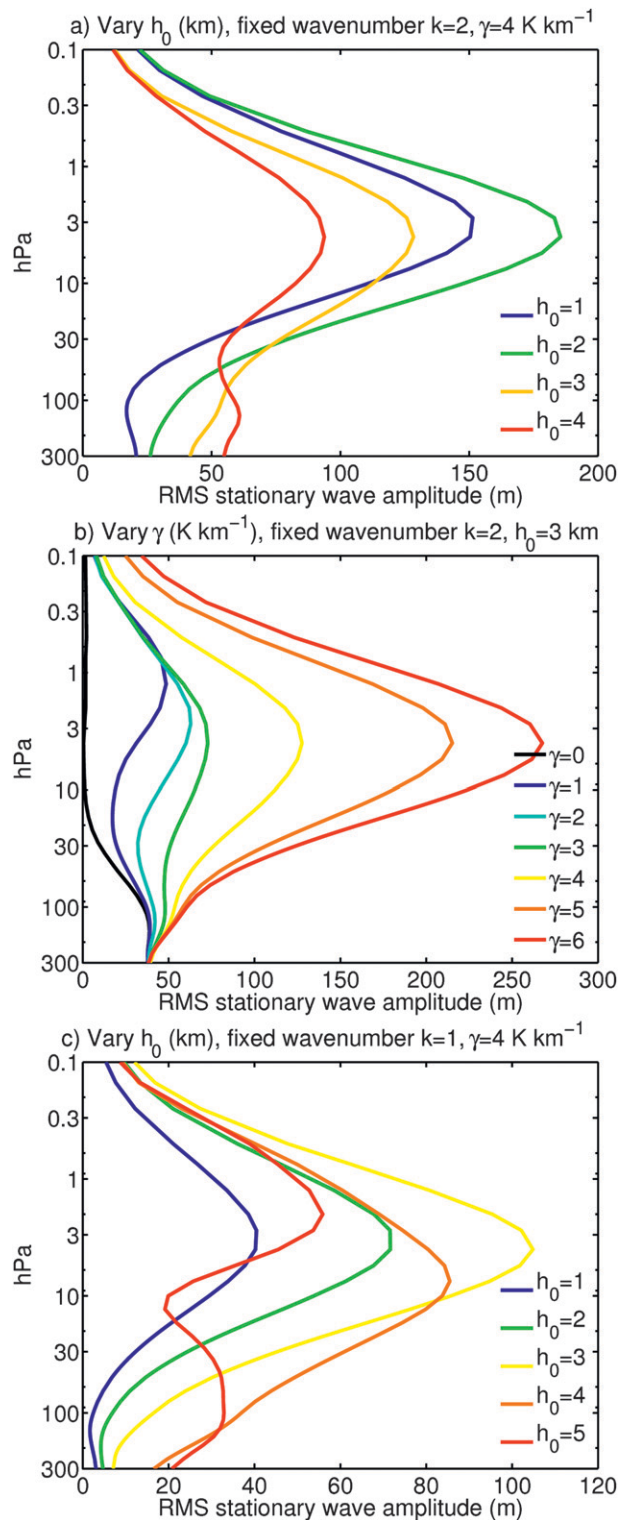

FIG. 6. The root-mean-square (RMS) stationary wave amplitude at 60°N, as a function of pressure, for integrations in which (a) h_0 is varied for wavenumber-2 topography and fixed $\gamma = 4$ K km^{-1} and (b) γ is varied for integrations with fixed wavenumber-2 topography of amplitude $h_0 = 3$ km. (c) As in (a), but for wavenumber-1 topography.
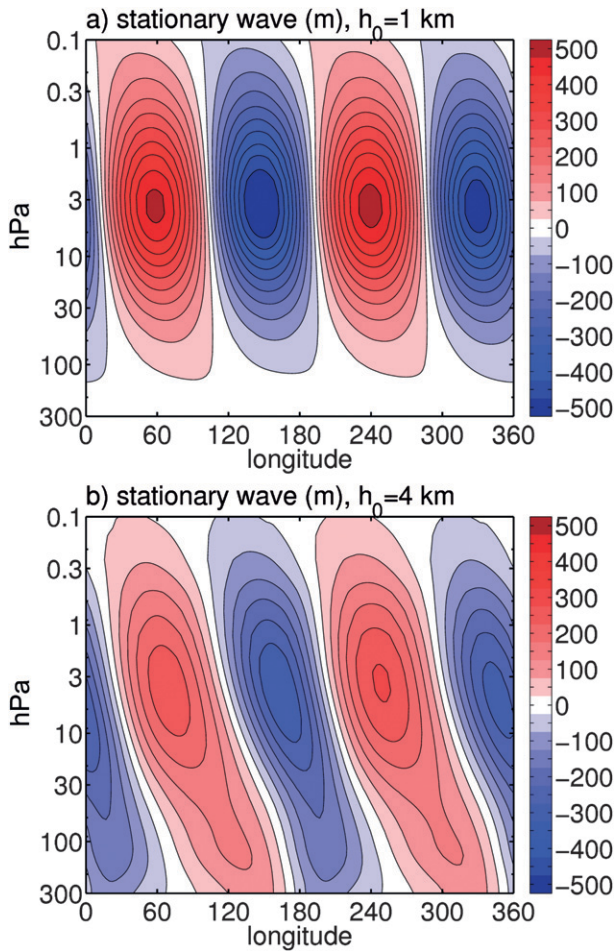
FIG. 7. The stationary wave structure at 60°N in two integrations with a cold vortex ($\gamma = 4$ K km^{-1}) and wavenumber-2 topography of amplitude (a) 1 and (b) 4 km.

Lindzen 2001). In Figs. 7a and 7b, we show the stationary waves for the integrations with $h_0 = 1$ and 4 km, respectively. For the latter integration, the stationary wave exhibits strong westward tilt with height, implying vertical propagation. This leads to strong wave breaking throughout the stratosphere, reducing the strength of the polar vortex. For the integration with weak topography, the wave amplitude increases considerably with height, reaching a maximum near 3 hPa, but the westward phase tilt is substantially diminished. The polar vortex in this simulation is much stronger (differences between these integrations are similar to those shown in Figs. 2a and 2c), forming a resonant cavity. Less wave activity is actually propagating upward, despite the increased amplitude of the wave.

We also explore the impact of different topographic structure. Wavenumber 1 has an impact similar to that of wavenumber 2, but the transmission of the wave from

the surface to the stratosphere is not as linear as for wavenumber-2 topography. As seen in Fig. 6c, for topography up to $h_0 = 3$ km, the stationary wave at the base of the stratosphere changes little, and only begins to increases substantially for larger values of h_0. As with wavenumber-2 topography, however, the wave forcing throughout the stratosphere scales with the wave amplitude at the base of the stratosphere (not shown). Wavenumbers 3 and 4, on the other hand, are very inefficient at driving the Brewer–Dobson circulation in the model, even at large amplitude. This behavior is consistent with the theoretical insight of Charney and Drazin (1961), who find that the strong winds in the polar vortex should inhibit the vertical propagation of smaller-scale stationary Rossby waves.

b. Stratospheric control

While diabatic forcing can generate a nonlinear Hadley circulation in the tropical stratosphere (e.g., Dunkerton 1989), mechanical forcing is necessary to maintain a circulation across angular momentum surfaces in the extratropics. In the absence of any mechanical driving, changes in the diabatic forcing of the extratropical stratosphere will simply result in a new equilibrium temperature, with no residual mean circulation (e.g., Andrews et al. 1987, 300–302). Hence the change in the circulation effected by the polar vortex lapse rate must be indirect, by modifying the behavior of the wave driving.

Charney and Drazin (1961) showed that while westerly winds are necessary for the propagation of a stationary Rossby wave, if the winds become too strong, the wave cannot maintain itself against downstream advection. The intrinsic easterly phase speed of a wave decreases with spatial scale (increased wavenumber), so as the winds increase, shorter wavelengths can no longer propagate vertically. Stratospheric wind velocities in the winter are sufficiently large that synoptic waves are inhibited, and only the gravest planetary waves have a chance of propagating in the vertical. Neglecting the horizontal structure of the winds, then, one might expect a colder vortex to suppress wave propagation. In the absence of topography, this intuition is correct. As found by Kushner and Polvani (2004, see their Fig. 3), the net wave flux into the upper stratosphere decreases with increasing γ in the model without topography.

In the presence of topography, however, Fig. 5 suggests that the vortex's influence on wave activity depends on altitude. Wave activity at 100 hPa is decreased when the vortex is cooled, but above 80 hPa, increasing γ allows more wave activity to propagate upward. The key lies in the meridional structure of the flow; γ induces a cooling of the polar vortex relative to the midlatitude and tropical stratosphere. Even for a very strong vortex,

however, there is always a region where wave propagation is possible.

The refractive index n^2 was introduced by Matsuno (1970) to account for the two-dimensional structure of the polar vortex. He derived a two-dimensional wave equation in the form $\xi_{zz} + \xi_{yy} + n^2\xi = 0$ for a wave quantity ξ. Wavelike solutions are possible when n^2 is positive, whereas only evanescent solutions exist when n^2 is negative. Following the formulation by Harnik and Lindzen (2001), we define n^2 by

$$n^2 = \left[\frac{\overline{q}_\phi}{r_0(\overline{u} - c)} - \left(\frac{k}{r_0 \cos\phi} \right)^2 - f^2 F(N^2) \right], \quad (6)$$

where $\overline{q}_\phi/r_0$ is the meridional gradient in potential vorticity:

$$\frac{\overline{q}_\phi}{r_0} = \overline{q}_y = \beta - \frac{1}{r_0^2}\left[\frac{(\overline{u}\cos\phi)_\phi}{\cos\phi} \right]_\phi + \frac{f^2}{R_d}\left(\frac{p\overline{\theta}}{T} \frac{\overline{u}_p}{\overline{\theta}_p} \right)_p. \quad (7)$$

The notation is standard, with r_0 being the radius of the earth, u the zonal wind, c and k the phase speed and zonal wavenumber of the wave, ϕ the latitude, $f = 2\Omega \sin\phi$ and β the Coriolis parameter and its meridional derivative, R_d the gas constant of dry air, p pressure, and θ and T the potential and standard temperatures. If N is constant, the function $F(N^2)$, detailed in Harnik and Lindzen (2001), reduces to $1/(2NH)^2$, where H is the scale height. While N is not constant in our model, we follow Simpson et al. (2009) and make this approximation, as $F(N^2)$ involves high-order derivatives of temperature, which lead to concerns about numerical accuracy. All results, however, are qualitatively the same if the full $F(N^2)$ is used.

Figure 8 illustrates the relationship between wave driving, as quantified by the divergence of the Eliassen–Palm flux, and the index of refraction for stationary waves ($c = 0$) of wavenumber 2 (the dominant wave forced by our surface topography) for three integrations with varying γ. On the left, we show the key elements that cause changes in n^2, the meridional potential vorticity gradient $\overline{q}_y$ and zonal mean zonal wind $\overline{u}$. In the case of no polar vortex, $\gamma = 0$ shown in Figs. 8a and 8b, the reduction in wave driving in the mid- to upper stratosphere can readily be understood in terms of the zero wind line across the lower stratosphere. Most waves break in the neighborhood of the critical line, and the diabatic circulation is very shallow. Note that the E-P flux divergence is shown in units of acceleration (force per unit mass), which emphasizes wave breaking at higher altitudes. As seen in Fig. 5d, the total wave forcing above 100 hPa is larger for $\gamma = 0$ than for $\gamma = 6$ K km^{-1}.

For a strong vortex, $\gamma = 6$ K km^{-1}, the net reduction of wave forcing is related to the throttle on wave propagation at the base of the stratosphere, the region of negative n^2 at 40°N and 100 hPa in Fig. 8f. Waves that get past this point through tunneling and changes in the index with time, however, experience a broader waveguide in the midstratosphere relative to the simulations with weak γ (Fig. 8d), particularly in the region of 10–50 hPa. The key differences are the strength of the potential vorticity gradients and width of the vortex, as seen by comparing Figs. 8c and 8e. The strong vortex creates a waveguide deeper into the stratosphere, allowing waves to propagate to higher altitudes.

While the index of refraction provides a qualitative explanation for the behavior of the model, it is important not to overinterpret results based on linear theory and the mean state. As shown in Fig. 2, the mean state is a function of both the wave driving and stratospheric thermal forcing. A given mean state does not uniquely describe the wave forcing; that is, a colder vortex can be obtained by cooling the stratosphere or reducing the stationary wave forcing from the troposphere. Since the index of refraction is based only on the mean state, it varies similarly when γ is fixed and the topography is varied (not shown). When the topography is changed, however, the index implies a false sense of causality. The vortex is weaker in cases of larger topography, which would suggest that there is less room for waves to propagate, but in this case the waveguide is weaker precisely because there is more wave breaking. The qualitative analysis based on the index of refraction only works if the wave driving at the base of the stratosphere is held fixed, as with the integrations shown in Fig. 8.

5. Connecting the diabatic circulation to tracer transport

Figure 5 shows that the changes in the diabatic circulation are driven by changes in wave driving in the winter hemisphere. To understand how these changes affect tracer transport, and so the differences in mean age observed in Fig. 1, we must connect the net mass circulation to tracer transport. Figures 9a and 9b illustrate the mean age of air at the equator as a function of h_0 and γ. The decrease in age with topography is fairly linear with h_0 at all levels, with some saturation at larger amplitudes. The relationship is more complicated for γ. The age is very sensitive for small values, particularly at upper levels, and then saturates at larger amplitudes. The integration with $\gamma = 0$ is singular in the upper stratosphere, as the residual circulation nearly vanishes above 10 hPa. Hence the age at 1 hPa was not nearly converged after almost 3 decades of integration.
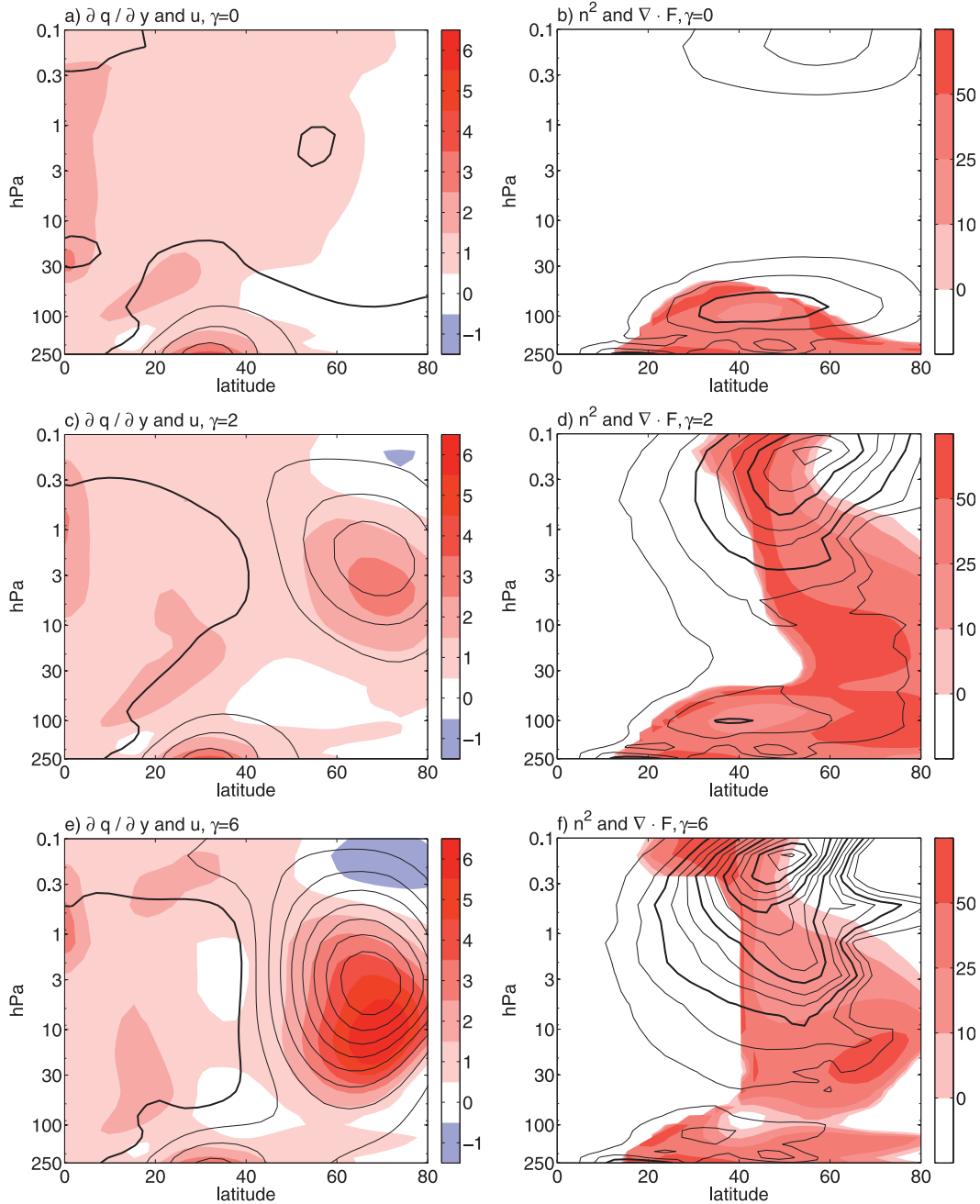
FIG. 8. The stratospheric waveguide for three integrations with varying polar vortex strength. (a),(c),(e) The potential vorticity gradient $\partial \overline{q}/\partial y$ (colors; units of β at 45°N) and the zonal mean wind (black contours; only positive winds are shown; the zero contour is thick, and the contour interval is 10 m s^{-1}). (b),(d),(f) The index of refraction (colors) and the divergence of the E-P flux [black contours; only negative values are shown and the thin (thick) contour interval is 0.5 (1.5) m s^{-1} day^{-1}]. All three integrations have wavenumber-2 topography of amplitude 3 km, and γ is (a),(b) 0, (c),(d) 2, and (e),(f) 6 K km^{-1}.

Figures 9c and 9d show net tropical upwelling as a function of h_0 and γ. As one would expect based on an advection–diffusion model (e.g., Waugh and Hall 2002), changes in upwelling tend to be the mirror image of

changes in age. For the case of varying topography, younger air is associated with greater upwelling. The situation is more complicated for changes in upwelling driven by γ, shown in Fig. 9d. The trends in upwelling
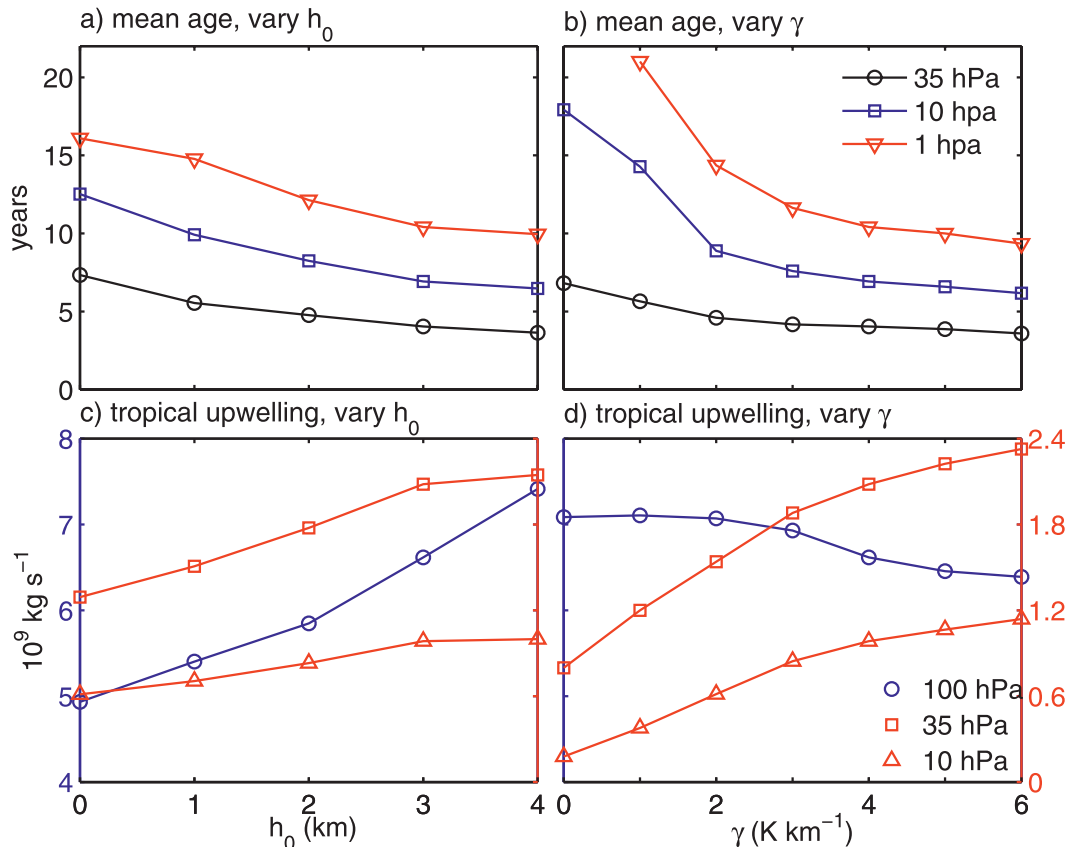
FIG. 9. Changes in (a),(b) the mean age of air at the equator and (c),(d) the total tropical upwelling as a function of (a),(c) the amplitude of wavenumber-2 topography with fixed vortex strength $\gamma = 4$ K km^{-1} and (b),(d) vortex strength γ with fixed topography ($k = 2$, $h_0 = 3$). Note the use of two vertical axes in (c) and (d): the left axis corresponds to 100-hPa upwelling, the right to the upwelling at 35 and 10 hPa.

mirror changes in age at upper levels (35 and 10 hPa), but at 100 hPa the tropical upwelling decreases at the same time as the age in the stratosphere above decreases.

Clearly, the net transport into the stratosphere (or across a particular pressure surface) may not be easily connected to the age. To highlight the relationship between age and the residual circulation, we show scatterplots of the residual velocity and the mean age in Fig. 10. Both panels show the relationship between the upwelling at the equator, which is a good proxy for the total tropical transport, with the age at the equator and 10 hPa. On the left, the plot is based on $\overline{\omega}^*$ at 100 hPa: as suggested by Fig. 9, there is significant scatter. Transport into the stratosphere is not correlated with the age across all of the integrations, exhibiting a correlation coefficient near zero. A linear relationship is found if one focusses only on changes associated with topography (blue squares), but the relationship is the opposite when γ is varied (red circles). Focusing on the upwelling at 28 hPa, however, as shown in Fig. 10b, one finds a fairly linear relationship

between age and upwelling across all the simulations, with a correlation coefficient $R = 0.98$. The slope of the scatter, approximately 1.5 yr (Pa day^{-1})$^{-1}$, quantifies the sensitivity of the age to changes in upwelling: a 1 Pa day^{-1} reduction in upwelling at 28 hPa leads to a 1.5-yr increase in mean age at 10 hPa. We note, however, that the age is quantitatively sensitive to model numerics, and so emphasize the qualitative link between age and upwelling reflected in the correlation coefficient.

Figure 10 highlights the fact that the relationship between the upwelling and the mean age at a given point depends on the structure of the residual circulation. By repeating this analysis for all points in latitude–pressure space (not shown) we find that the age in the middle and upper stratosphere depends critically on the depth of upwelling in the tropics, even for points in the high latitudes. Mixing along quasi-horizontal isentropes can efficiently transport tracers to the higher latitudes, but it can only act if the tracer is brought sufficiently high into the stratosphere by the diabatic circulation in the tropics.
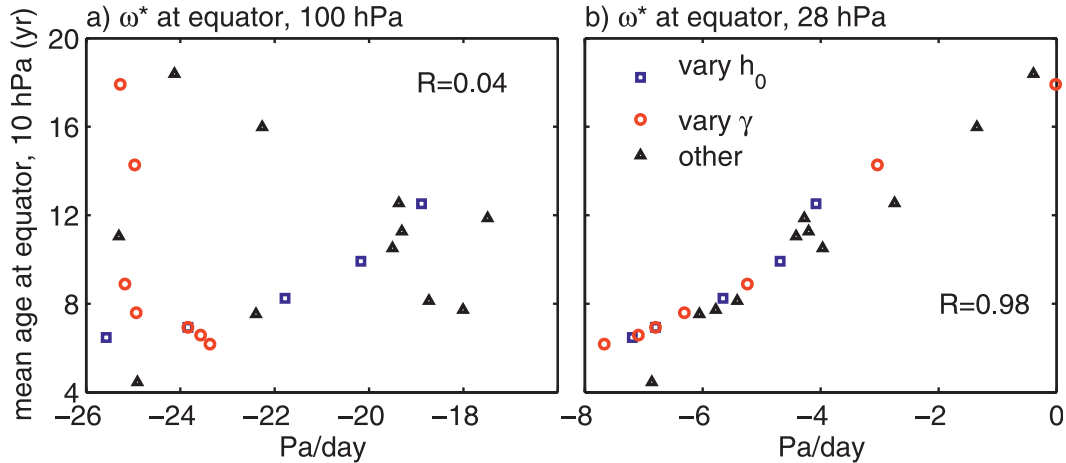
FIG. 10. Scatterplots showing the relationship between the mean age of air at the equator and 10 hPa with the residual mean velocity at the equator and (a) 100 and (b) 28 hPa. The blue and red symbols highlight the integrations in which h_0 and γ are varied, respectively, as shown in Fig. 9.

Thus far we have focused primarily on the mean age. As shown in the left and middle columns of Fig. 11, other properties of the age spectrum largely follow the mean age. In the left column, we show the spectral width for the four key integrations shown in Figs. 1–3. The width is substantially larger in the two "old" integrations, where there is no topography or the vortex is very weak. The spectral width is largest in the lower stratosphere, particularly for the integration with $\gamma = 4$ K km^{-1} and $h_0 = 0$ (Fig. 11a), suggesting a wide variation in how parcels reach this region, faster through mixing from the troposphere, or slower along trajectories through the deep circulation high into the stratosphere. The spectral width is slightly smaller in the other old integration, with $\gamma = 1.5$ K km^{-1} and $h_0 = 3000$ m (Fig. 11d). The modal age in the winter stratosphere, however, is slightly larger in this integration, as shown in the middle column of Fig. 11. Parcels are more slowly advected up into the upper stratosphere, but there is less variance in the trajectories. The two effects cancel each other out, so that the two old integrations have about the same mean age in the upper stratosphere.

The modal age highlights the potential isolation of air over the pole by the stratospheric polar vortex. The modal age is higher in the lower polar stratosphere (~50 hPa) in the integrations shown in Figs. 11b and 11k, despite the fact that their mean age is quite different. As shown in Fig. 2, the unifying element in these two integrations is the strength of the polar vortex. A strong polar night jet leads to enhanced potential vorticity gradients on the vortex edge, which in turn inhibits mixing along isentropic surfaces (e.g., Bühler and Haynes 1999; Sobel and Plumb 1999). In these integrations,

then, mass transport in the vortex is dominated by the slow, deep circulation from above.

The impact of the vortex on mixing along isentropes is more clearly visible in the meridional gradient of the mean age, shown in the right column of Fig. 11. Gradients in the mean age reveal transport barriers in the stratosphere. In all integrations, there is evidence of the two main barriers to transport, separated by a well-mixed "surf zone" between roughly 30° and 60° (e.g., McIntyre and Palmer 1983; Plumb 2002). The tropical barrier, centered near 20°, is the most prominent, but a secondary barrier on the edge of the polar vortex is visible at 70° in all integrations. The strength of the transport barriers in the winter hemisphere, however, is not well correlated with the mean age. The barriers are strongest in the old integration with $\gamma = 4$ K km^{-1} and $h_0 = 0$ (Fig. 11c) and the "young" integration with $\gamma = 5$ K km^{-1} and $h_0 = 3000$ m (Fig. 11l). As with the modal age discussed above, the key unifying factor in these integrations is the strength of the polar vortex. As shown in Fig. 8, potential vorticity gradients are increased on both sides of the surf zone when the vortex is stronger, inhibiting mixing.

The age of air in the mid- to upper stratosphere depends critically on the ability of the diabatic circulation to bring mass up from the lower stratosphere. It is thus controlled by the "deep" branch of the residual mean circulation, and so is equally sensitive to changes in wave forcing and the diabatic forcing of the stratosphere. Mixing along isentropic surfaces, however, is sensitive to the strength of potential vorticity gradients and plays an important role in ventilating the lower polar stratosphere.
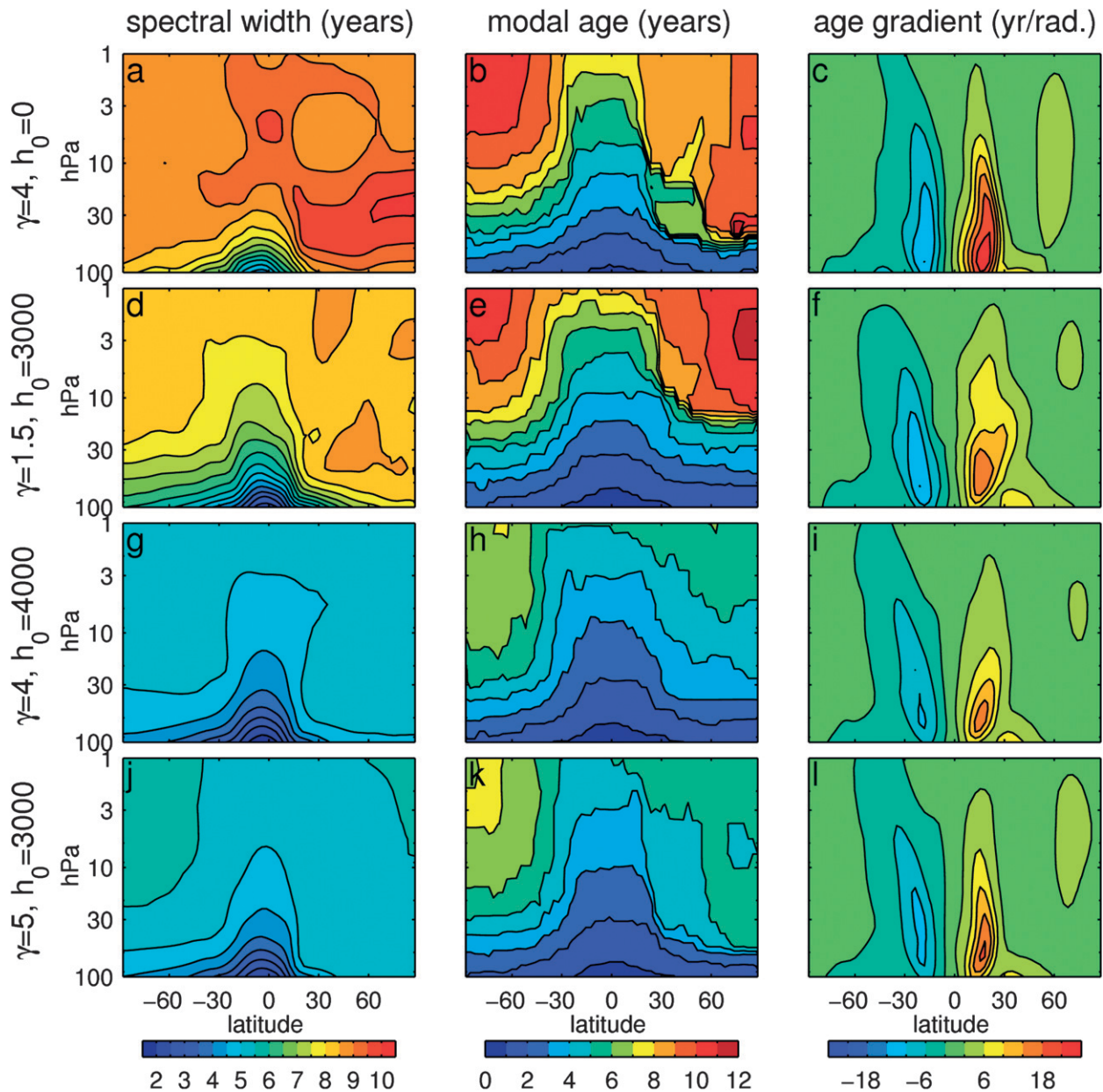
FIG. 11. Properties of the age spectrum for the four integrations shown in Figs. 1–3. (a)–(f) The ''old'' integrations and (g)–(l) the ''young'' integrations. (left) The width of the age spectrum, (middle) the modal age, and (right) the meridional gradient of the mean age. Note that the parameter h_0 is specified in m.

6. Impacts on the tropopause and cold point

By focusing on the age of the air, we have emphasized the impact of the stratospheric circulation on the tracer transport, which is most directly relevant to stratospheric ozone chemistry. The Brewer–Dobson circulation can also impact tropospheric climate by shaping the tropopause (Birner 2010) and altering the water vapor content of the stratosphere by modulating the temperature of the tropical cold point (e.g., Mote et al. 1996; Solomon et al. 2010).

Figure 12 quantifies changes in the tropopause height, as defined with the conventional World Meteorological Organization (WMO) criteria, the level at which the lapse rate is -2 K km^{-1}. Figures 12a and 12b show that increased topography raises the tropopause in the tropics. By increasing the diabatic circulation in the upper troposphere and lower stratosphere (UTLS), topography cools this region of the atmosphere in the tropics and warms it in the extratropics. According to the theory of the tropopause height developed by Held
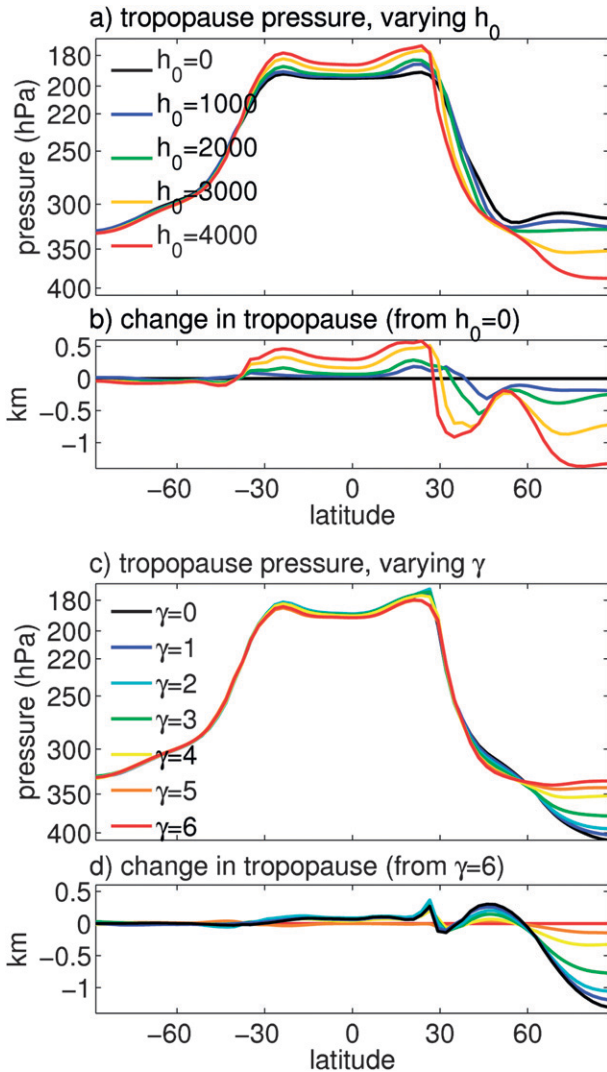
FIG. 12. The impact of (a) topographic amplitude and (c) vortex strength on the location of the tropopause. (b),(d) The corresponding changes in the tropopause height. In (a) and (b), all integrations have wavenumber-2 topography with fixed $\gamma = 4$ K km^{-1}. In (c) and (d), the topography is fixed, with wavenumber 2 and amplitude 3 km.

(1982), a cooling (warming) of the lower stratosphere will induce the tropospheric circulation to deepen (shallow) in order to keep the troposphere in net radiative equilibrium [see also Vallis (2006), ch. 12]. The model suggests that a substantial change in the equator-to-pole gradient of the tropopause height (on the order of 1 km) can be effected by increasing the BDC in the lower stratosphere, consistent with the calculations of Birner (2010). Changes in γ, shown in Figs. 12c and 12d, have a smaller effect on the tropical tropopause. When γ is decreased, there is a small rise in the tropical tropopause due to increased upwelling. There are more significant
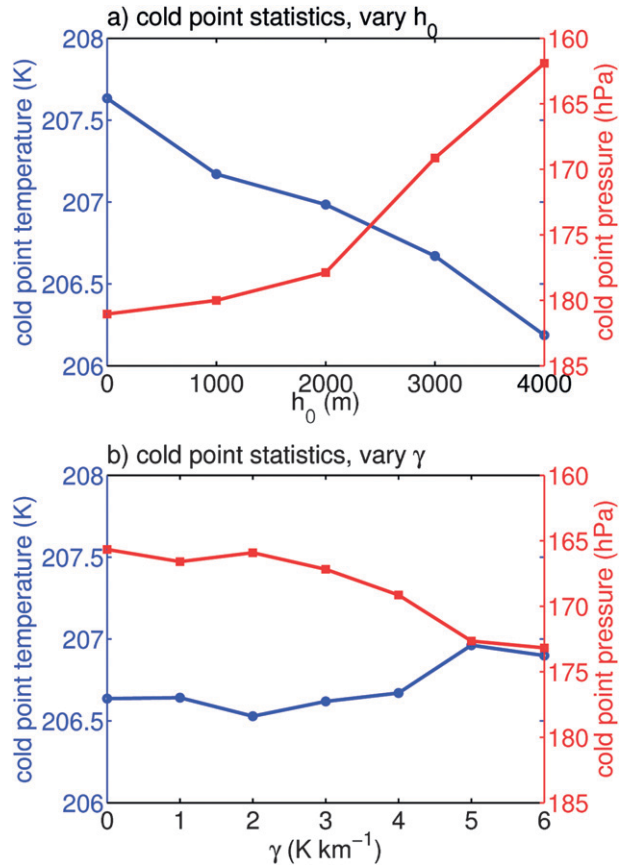

FIG. 13. The impact of (a) topographic amplitude and (b) vortex strength on the temperature and location of the cold point. The cold point is defined by the minimum temperature in the tropics, averaged between 10°S and 10°N.

impacts in the extratropics, where warming of the vortex lowers the tropopause at the pole by over a kilometer. This is driven in part by local changes in downwelling, as seen in Fig. 4d.

We note, however, that the distinction between the tropopause height in the tropics and extratropics is well established in integrations with no topography or weak γ. Haqq-Misra et al. (2011) document the impact of synoptic eddies on the shallow branch of the Brewer–Dobson circulation, which play a significant role in establishing the contrast between the tropics and extratropics. Here we find that changes in the circulation driven by planetary-scale waves can also increase the contrast.

Figure 13 illustrates changes in the cold point temperature and pressure induced by varying topographic and stratospheric vortex forcing. The results are closely related to changes in the tropical tropopause height. Figure 13a shows that increased upwelling driven by changes in planetary waves can cool the cold point (on the order of a degree) and raise it higher in the stratosphere (on the order

of 10 hPa). Changes in response to γ are more subtle, on the order of half a degree. This response is driven by the slight weakening of the tropical upwelling in response to a colder vortex.

The model integrations suggest that tropospheric control on the wave forcing plays the largest role in the impact of the Brewer–Dobson circulation on the tropopause and cold point. These metrics are most sensitive to the shallow branch of the BDC, and so less dependent on conditions in the polar vortex above. This has implications for our understanding of the seasonal cycle of these features, as discussed in the context of idealized GCMs by Chen and Sun (2011). They found that the annual cycle of the BDC at 70 hPa was well captured by integrations in which the forcing was varied seasonally in the stratosphere alone, but that at 100 hPa and below the seasonal forcing of the troposphere became more important.

The seasonal cycle in the stratosphere is most readily connected to γ, with strong values corresponding to winter and weaker values to summer. As shown in Fig. 5b, changes in γ have a strong impact above 80 hPa: the diabatic circulation is increased when the polar vortex is colder, as in the winter. As the planetary wave forcing is stronger in the NH, Chen and Sun (2011) show that the diabatic circulation is thus strongest in boreal winter, which is in turn reflected in colder lower-stratospheric temperatures (e.g., Yulaeva et al. 1994; Rosenlof 1995).

The tropical cold point, however, is lower in the atmosphere, below the level where changes in the polar vortex (stratospheric control) have a strong impact in our model. At this level, the seasonal impact of the polar vortex would actually appear to be reversed: a colder vortex is associated with weaker upwelling and a warmer cold point. Rather, the integrations suggest that changes in tropospheric wave driving are needed to drive the seasonal cycle at these levels—although we do not claim that changes in planetary wave activity are the dominant mechanism behind the seasonal cycle. Randel et al. (2008) find that changes in subtropical wave driving are essential to understanding seasonal variations in tropical upwelling at 100 hPa, and depend on waves originating in both the tropics and extratropics.

7. Structural changes in the Brewer–Dobson circulation

Several recent studies have investigated changes in the BDC in response to anthropogenic forcing. Comprehensive models universally predict an increase of the circulation at all heights (e.g., Butchart and Scaife 2001; Li et al. 2008; Garcia and Randel 2008; McLandress and Shepherd 2009). Engel et al. (2009) do not find evidence of a strengthening trend based on observations over the

past 3 decades, but the uncertainty in measurements is sufficiently large that model trends cannot be ruled out. Bönisch et al. (2011) suggest that differences between observations and models could be related to structural changes in the BDC. Specifically, they argue that an increase in the overturning in the lower stratosphere could explain model results, while a slowing (or lack of a change) in the deep overturning could keep the mean age in the mid- to upper stratosphere from decreasing.

Our model integrations confirm that such structural changes in the circulation are possible, illustrating that transport in the lower stratosphere can vary independently of transport in the middle to upper stratosphere. The mechanism lies in the relative independence of the stratospheric and tropospheric controls of the circulation. As illustrated in Fig. 14, by reducing γ (warming the polar vortex) while increasing h_0 (increasing the tropospheric wave forcing), the diabatic circulation in the lower stratosphere increases simultaneously with the mean age in the mid- and upper stratosphere. The increased wave forcing strengthens the overall circulation, but the weakening of the polar vortex lowers the breaking level of the waves, resulting in a shallower circulation. We strongly emphasize, however, that this result only suggests the possibility that the paradoxical trends in models and observations could be due to structural changes. Garcia et al. (2011) show that sampling limitations in observations leads to significant uncertainty, and it is quite possible that the apparent contradiction between models and observations is due to limitations on available measurements.

8. Conclusions

We have explored factors that control the strength and structure of the Brewer–Dobson circulation in an idealized general circulation model, linking changes in the net circulation of mass to changes in tracer transport. We have shown that the diabatic forcing of the stratospheric polar vortex and planetary wave forcing by the troposphere can have comparable effects on the mean age of air in the mid- to upper stratosphere. Their impact on the age, however, is mediated through different controls on the diabatic circulation. Increased planetary wave forcing leads to an overall increase in the strength of the BDC, particularly the lower branch of the circulation, an effect we term "tropospheric control." A colder polar vortex, on the other hand, creates a waveguide higher into the stratosphere, raising the breaking level of the planetary waves and deepening the circulation, an effect we term "stratospheric control." Ventilation of mass in the mid- to upper stratosphere depends critically on penetration of tropical upwelling deep into the stratosphere,
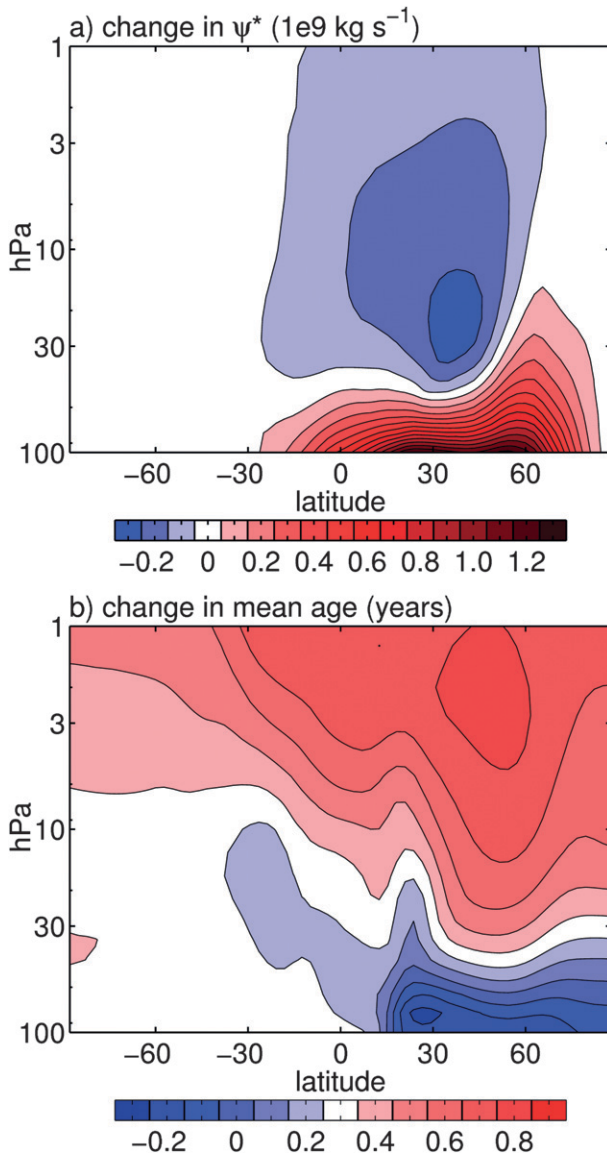
FIG. 14. The potential for structural change in the Brewer–Dobson circulation. The difference in (a) the residual mean mass streamfunction and (b) the mean age of air, between integrations 16 and 3, showing the impact of increasing the stationary wave forcing (increasing h_0 from 2 to 3 km) while simultaneously warming the polar vortex (reducing γ from 4 to 2 K km^{-1}). With coordinated changes in the forcing, it is possible to increase the circulation at lower levels while increasing the age at upper levels.

and so the age of air is comparably sensitive to both tropospheric and stratospheric controls. The relative independence of the physical processes underlying tropospheric wave driving and stratospheric diabatic forcing provide a pathway for structural changes in the Brewer–Dobson circulation, as suggested in recent observations by Bönisch et al. (2011).

The tropospheric wave driving was modified by varying the amplitude and structure of idealized topography at the surface, as in Gerber and Polvani (2009). We found that wave breaking though the depth of the stratosphere is well correlated with the amplitude of stationary, planetary-scale waves 1 and 2 at the base of the stratosphere. The relationship between wave amplitude and wave breaking in the stratosphere, however, is highly nonlinear. In the stratosphere, stationary wave amplitude depends more critically on the strength of the polar vortex, as a strong polar vortex sets up a resonant cavity and increases wave reflection. Reflection can lead to large stationary waves with little vertical phase tilt, and consequently little propagation of wave activity.

The thermal structure of the stratosphere was altered by varying the parameter γ of the Polvani and Kushner (2002) model, the lapse rate of the equilibrium temperature profile in the winter hemisphere. A colder equilibrium profile leads to a stronger polar night jet. Outside the tropics, the diabatic forcing cannot directly force the Brewer–Dobson circulation, and so can only affect it indirectly by modifying the wave breaking. The theoretical work of Charney and Drazin (1961) suggests that a stronger vortex will limit Rossby wave propagation into the stratosphere, thus reducing the amplitude of the Brewer–Dobson circulation. In the lower stratosphere this provides the correct intuition: the net wave forcing of the stratosphere is reduced when the vortex is colder, especially when there is no stationary wave forcing in the lower stratosphere, as explored by Kushner and Polvani (2004). At upper levels, however, wave breaking increases with a colder vortex, as potential vorticity gradients along the edge of the vortex create a waveguide higher into the stratosphere.

The mean age of air in the mid- and upper stratosphere depends primarily on the deep branch of the Brewer–Dobson circulation, the upwelling of air high into the stratosphere. It is therefore sensitive to both changes in planetary waves forcing from the troposphere and the diabatic forcing of the stratosphere. Younger air is associated with a narrower spectral width, which signifies less variance in the tracer trajectories, and a reduced modal age, suggesting more direct transport. Tracer transport into the lower polar stratosphere, however, is also sensitive to the strength of polar vortex, as strong potential vorticity gradients inhibit mixing along isentropes, isolating the polar air.

The tropopause and tropical cold point, on the other hand, depend primarily on the shallow Brewer–Dobson circulation and thus are most sensitive to changes in wave forcing from the troposphere. This result has implications for our understanding of the seasonal cycle of the BDC in the lower stratosphere. As shown by Chen

and Sun (2011), seasonal changes in the polar vortex strength (stratospheric control) drive the seasonal evolution of tropical upwelling at 70 hPa and above by modulating the depth of the wave penetration. Below this layer, however, changes in tropospheric wave driving (tropospheric control) become dominant, as found by Randel et al. (2008).

In using an idealized GCM, we have neglected the important impact of small-scale gravity waves on the Brewer–Dobson circulation. Preliminary work with orographic and nonorographic gravity wave parameterizations in the model, however, indicates that our main conclusions are robust. Changes induced by parameterization of gravity waves are in fact partially compensated by equal and opposite changes in the resolved waves, leaving less impact on the BDC than might be expected. We have also investigated the impact of model resolution and numerics on our conclusions. While the structure of the diabatic circulation is very robust to changes in resolution and numerics, the quantitative properties of tracer transport is not, consistent with analysis of a more comprehensive chemistry–climate model by Eluszkiewicz et al. (2000). Hence we have focused on qualitative changes in the tracer transport in this paper. Results on the robustness to both numerics and gravity wave parameterization will be documented in future publications.

REFERENCES

Andrews, D. G., and M. E. McIntyre, 1976: Planetary waves in horizontal and vertical shear: The generalized Eliassen–Palm relation and the mean zonal acceleration. *J. Atmos. Sci.,* **33,** 2031–2048.

——, J. R. Holton, and C. B. Leovy, 1987: *Middle Atmosphere Dynamics.* Academic Press, 489 pp.

Arblaster, J. M., and G. A. Meehl, 2006: Contributions of external forcings to southern annular mode trends. *J. Climate,* **19,** 2896–2905.

Birner, T., 2010: Residual circulation and the tropopause structure. *J. Atmos. Sci.,* **67,** 2582–2600.

——, and H. Bönisch, 2011: Residual circulation trajectories and transit times into the extratropical lowermost stratosphere. *Atmos. Chem. Phys.,* **11,** 817–827.

Bönisch, H., A. Engel, T. Birner, P. Hoor, D. W. Tarasick, and E. A. Ray, 2011: On the structural change in the Brewer–Dobson circulation after 2000. *Atmos. Chem. Phys.,* **11,** 3937–3948.

Brewer, A. W., 1949: Evidence for a world circulation provided by the measurements of helium and water vapour distribution in the stratosphere. *Quart. J. Roy. Meteor. Soc.,* **75,** 351–363.

Bühler, O., and P. H. Haynes, 1999: Constraints on the mean mass transport across potential vorticity contours. *J. Atmos. Sci.,* **56,** 942–947.

Butchart, N., and A. A. Scaife, 2001: Removal of chlorofluorocarbons by increased mass exchange between the stratosphere and troposphere in a changing climate. *Nature,* **410,** 799–802.

Charney, J. G., and P. G. Drazin, 1961: Propagation of planetary-scale disturbances from the lower into the upper atmosphere. *J. Geophys. Res.,* **66,** 83–109.

Chen, G., and L. Sun, 2011: Mechanisms of the tropical upwelling branch of the Brewer–Dobson circulation: The role of extratropical waves. *J. Atmos. Sci.,* **68,** 2878–2892.

Dobson, G. M. B., 1956: Origin and distribution of polyatomic molecules in the atmosphere. *Proc. Roy. Soc. London,* **A236,** 187–193.

——, D. N. Harrison, and J. Lawrence, 1929: Measurements of the amount of ozone in the earth's atmosphere and its relation to other geophysical conditions—Part III. *Proc. Roy. Soc. London,* **A122,** 456–486.

Dunkerton, T. J., 1989: Nonlinear Hadley circulation driven by asymmetric differential heating. *J. Atmos. Sci.,* **46,** 956–974.

Edmon, H. J., B. J. Hoskins, and M. E. McIntyre, 1980: Eliassen–Palm cross sections for the troposphere. *J. Atmos. Sci.,* **37,** 2600–2616.

Eluszkiewicz, J., R. S. Hemler, J. D. Mahlman, L. Bruhwiler, and L. L. Takacs, 2000: Sensitivity of age-of-air calculations to the choice of advection scheme. *J. Atmos. Sci.,* **57,** 3185–3201.

Engel, A., and Coauthors, 2009: Age of stratospheric air unchanged within uncertainties over the past 30 years. *Nat. Geosci.,* **2,** 28–31, doi:10.1038/ngeo388.

Eyring, V., T. G. Shepherd, and D. W. Waugh, Eds., 2010: SPARC Report on the Evaluation of Chemistry Climate Models. SPARC Rep. 5, WCRP-30, WMO/TD 1526. [Available online at http://www.sparc-climate.org/publications/sparc-reports/sparc-report-no5/.]

Garcia, R. R., and W. J. Randel, 2008: Acceleration of the Brewer–Dobson circulation due to increases in greenhouse gases. *J. Atmos. Sci.,* **65,** 2731–2739.

——, ——, and D. E. Kinnison, 2011: On the determination of age of air trends from atmospheric trace species. *J. Atmos. Sci.,* **68,** 139–154.

Gerber, E. P., and L. M. Polvani, 2009: Stratosphere–troposphere coupling in a relatively simple AGCM: The importance of stratospheric variability. *J. Climate,* **22,** 1920–1933.

Hall, T. M., and R. A. Plumb, 1994: Age as a diagnostic of stratospheric transport. *J. Geophys. Res.,* **99,** 1059–1070.

——, D. W. Waugh, K. A. Boering, and R. A. Plumb, 1999: Evaluation of transport in stratospheric models. *J. Geophys. Res.,* **104,** 18 815–11 839.

Haqq-Misra, J., S. Lee, and D. M. W. Frierson, 2011: Tropopause structure and the role of eddies. *J. Atmos. Sci.,* **68,** 2930–2944.

Harnik, N., and R. S. Lindzen, 2001: The effect of reflecting surfaces on the vertical structure and variability of stratospheric planetary waves. *J. Atmos. Sci.,* **58,** 2872–2894.

Haynes, P. H., C. J. Marks, M. E. McIntyre, T. G. Shepherd, and K. P. Shine, 1991: On the "downward control" of extratropical diabatic circulations by eddy-induced mean zonal forces. *J. Atmos. Sci.,* **48,** 651–678.

Held, I. M., 1982: On the height of the tropopause and the static stability of the troposphere. *J. Atmos. Sci.,* **39,** 412–417.

——, and M. J. Suarez, 1994: A proposal for the intercomparison of the dynamical cores of atmospheric general circulation models. *Bull. Amer. Meteor. Soc.,* **75,** 1825–1830.

——, and T. Schneider, 1999: The surface branch of the zonally averaged mass transport circulation in the troposphere. *J. Atmos. Sci.,* **56,** 1688–1697.

Holton, J. R., P. H. Haynes, M. E. McIntyre, A. R. Douglass, R. B. Rood, and L. Pfister, 1995: Stratosphere–troposphere exchange. *Rev. Geophys.,* **33,** 403–439.

Kushner, P. J., and L. M. Polvani, 2004: Stratosphere–troposphere coupling in a relatively simple AGCM: The role of eddies. *J. Climate,* **17,** 629–639.

Li, F., J. Austin, and J. Wilson, 2008: The strength of the Brewer–Dobson circulation in a changing climate: Coupled chemistry–climate model simulations. *J. Climate,* **21,** 40–57.

Matsuno, T., 1970: Vertical propagation of stationary planetary waves in the winter Northern Hemisphere. *J. Atmos. Sci.,* **27,** 871–883.

McIntyre, M. E., and T. N. Palmer, 1983: Breaking planetary waves in the stratosphere. *Nature,* **305,** 593–600.

McLandress, C., and T. G. Shepherd, 2009: Impact of climate change on stratospheric sudden warmings as simulated by the Canadian Middle Atmosphere Model. *J. Climate,* **22,** 5449–5463.

——, ——, J. F. Scinocca, D. A. Plummer, M. Sigmond, A. I. Jonsson, and M. C. Reader, 2011: Separating the dynamical effects of climate change and ozone depletion. Part II: Southern Hemisphere troposphere. *J. Climate,* **24,** 1850–1868.

Mote, P. W., and Coauthors, 1996: An atmospheric tape recorder: The imprint of tropical tropopause temperatures on stratospheric water vapor. *J. Geophys. Res.,* **101,** 3989–4006.

Perlwitz, J., S. Pawson, R. Fogt, J. E. Nielsen, and W. Neff, 2008: The impact of stratospheric ozone hole recovery on Antarctic climate. *Geophys. Res. Lett.,* **35,** L08714, doi:10.1029/2008GL033317.

Plumb, R. A., 2002: Stratospheric transport. *J. Meteor. Soc. Japan,* **80,** 793–809.

Polvani, L. M., and P. J. Kushner, 2002: Tropospheric response to stratospheric perturbations in a relatively simple general circulation model. *Geophys. Res. Lett.,* **29,** 1114, doi:10.1029/2001GL014284.

——, D. W. Waugh, G. J. P. Correa, and S.-W. Son, 2011: Stratospheric ozone depletion: The main driver of twentieth-century atmospheric circulation changes in the Southern Hemisphere. *J. Climate,* **24,** 795–812.

Randel, W. J., R. Garcia, and F. Wu, 2008: Dynamical balances and tropical stratospheric upwelling. *J. Atmos. Sci.,* **65,** 3584–3595.

Rosenlof, K. H., 1995: Seasonal cycle of the residual mean meridional circulation in the stratosphere. *J. Geophys. Res.,* **100,** 5173–5191.

Shaw, T. A., M. Sigmond, T. G. Shepherd, and J. F. Scinocca, 2009: Sensitivity of simulated climate to conservation of momentum in gravity wave drag parameterization. *J. Climate,* **22,** 2726–2742.

Shepherd, T. G., and T. A. Shaw, 2004: The angular momentum constraint on climate sensitivity and downward influence in the middle atmosphere. *J. Atmos. Sci.,* **61,** 2899–2908.

Simpson, I. R., M. Blackburn, and J. D. Haigh, 2009: The role of eddies in driving the tropospheric response to stratospheric heating perturbations. *J. Atmos. Sci.,* **66,** 1347–1365.

Sobel, A., and R. A. Plumb, 1999: Quantitative diagnostics of mixing in a shallow water model of the stratosphere. *J. Atmos. Sci.,* **56,** 2811–2829.

Solomon, S., K. H. Rosenlof, R. W. Portmann, J. S. Daniel, S. M. Davis, T. J. Sanford, and G.-K. Plattner, 2010: Contributions of stratospheric water vapor to decadal changes in the rate of global warming. *Science,* **327,** 1219–1223.

Son, S.-W., and Coauthors, 2008: The impact of stratospheric ozone recovery on the Southern Hemisphere westerly jet. *Science,* **320,** 1486–1489, doi:10.1126/science.1155939.

Thompson, D. W. J., and S. Solomon, 2002: Interpretation of recent Southern Hemisphere climate change. *Science,* **296,** 895–899.

Vallis, G. K., 2006: *Atmospheric and Oceanic Fluid Dynamics.* Cambridge University Press, 745 pp.

Waugh, D. W., and T. M. Hall, 2002: Age of stratospheric air: Theory, observations, and models. *Rev. Geophys.,* **40,** 1010, doi:10.1029/2000RG000101.

Yulaeva, E., J. R. Holton, and J. M. Wallace, 1994: On the cause of the annual cycle in tropical lower-stratospheric temperatures. *J. Atmos. Sci.,* **51,** 169–174.